Bulletin of Pure and Applied Sciences.
Vol.38 D (Physics), No.2,
July-December 2019 P. 94-107

Print version ISSN 0970 6569
Online version ISSN 2320 3218
DOI: 10.5958/2320-3218.2019.00015.0

Original Research Article

Available online at www.bpasjournals.com

Shape Coexistence in the Entrance Channel of Heavy-Ion Fusion: Coupled-Channels Calculations for Prolate, Oblate, and Spherical Minima

Dr. Rahul Kumar[1]

Author's Affiliations:

Dr. Rahul Kumar [1]Assistant Professor (GT), Department of Physics, H.R. College, Amnour (Saran),
Jai Prakash University, Chapra (Saran), Bihar, India
Email: rahul.nishu@yahoo.com

***Corresponding author:** **Dr. Rahul Kumar**
Assistant Professor (GT), Department of Physics, H.R. College, Amnour (Saran),
Jai Prakash University, Chapra (Saran), Bihar, India
Email: rahul.nishu@yahoo.com

ABSTRACT Heavy-ion fusion at energies near and below the Coulomb barrier provides one of the most sensitive probes of nuclear structure available in low-energy nuclear physics. The coupling between the relative motion of the colliding nuclei and the intrinsic degrees of freedom of target and projectile is known to enhance sub-barrier fusion cross sections by orders of magnitude and to redistribute a single barrier into a characteristic distribution of barriers. In a growing number of nuclei across the chart, low-lying prolate, oblate, and spherical minima coexist within an energy window of a few hundred keV, so that the colliding system does not possess a single well-defined intrinsic shape in the entrance channel. This article develops a coupled-channels description in which the entrance channel couples simultaneously to several coexisting intrinsic configurations, each carrying its own collective band, and in which configuration mixing transfers strength between them. The formalism is built on the standard eigenchannel reduction of the coupled-channels equations and is used to compute fusion excitation functions, barrier distributions, and mean angular momenta for representative medium-mass and heavy systems. The results demonstrate that prolate, oblate, and spherical entrance configurations leave distinct fingerprints on the barrier distribution, that configuration mixing shifts the effective barrier centroid downward and smooths the distribution, and that the largest sub-barrier enhancement is obtained when all three minima participate coherently. These findings establish entrance-channel shape coexistence as a measurable contributor to sub-barrier fusion dynamics and clarify how multi-configuration structure must be incorporated into quantitative fusion calculations.

KEYWORDS Shape coexistence, Heavy-ion fusion, Coupled channels, Barrier distribution, Intrinsic configurations, Sub-barrier enhancement.

INTRODUCTION

The fusion of two atomic nuclei at energies in the vicinity of the Coulomb barrier is governed by quantum-mechanical tunnelling through a potential barrier formed by the competition between the long-range Coulomb repulsion and the short-range nuclear attraction [1]. Early measurements established that the experimental fusion cross sections at sub-barrier energies exceed the predictions of a one-dimensional barrier-penetration model by factors ranging from several to many orders of magnitude [2]. This enhancement is now understood to arise from the coupling of the relative motion of the colliding nuclei to their internal degrees of freedom, including collective surface vibrations, static deformation, and nucleon-transfer channels [3, 4]. The systematic study of these couplings has matured into one of the central themes of low-energy nuclear reaction physics, and it provides a uniquely sensitive window onto the structure of the participating nuclei [5]..

A decisive conceptual advance was the recognition that the effect of channel coupling can be represented, in the limit where the intrinsic excitation energies are small compared with the curvature of the barrier, as a distribution of barriers rather than a single barrier [6]. The distribution of barriers can be extracted experimentally as the second derivative of the energy-weighted fusion cross section with respect to the centre-of-mass energy, and it constitutes a remarkably direct fingerprint of the entrance-channel structure [7]. High-precision excitation functions measured over the past decades have confirmed that static quadrupole and hexadecapole deformation, single- and multi-phonon vibrational excitations, and positive-Q-value transfer channels each imprint a recognizable structure on the barrier distribution [8, 9]. The theoretical framework that underlies these analyses is the coupled-channels method, in which the Schrödinger equation for the relative motion is solved simultaneously with equations describing the intrinsic excitations, retaining couplings to all orders in the deformation [10]. Comprehensive reviews of the field document the steady refinement of both the experimental techniques and the coupled-channels calculations that interpret them [19, 20, 21].

Independently of the reaction-physics developments, nuclear-structure studies have established that many nuclei do not possess a single well-defined ground-state shape. Instead, several distinct intrinsic configurations, associated with different minima of the deformation energy surface, may coexist at low excitation energy [11]. This phenomenon of shape coexistence has been observed across the nuclear chart and is now recognized as a general feature of finite nuclear many-body systems [12]. The coexistence of weakly oblate and strongly prolate shapes has been documented in the neutron-deficient mercury isotopes [13], and the simultaneous occurrence of spherical, prolate, and oblate 0^+ states within a narrow energy interval has been established in ^{186}Pb, which remains the cleanest example of triple shape coexistence [14]. In the mass-70 region around $N \approx Z$, rapid changes of shape with nucleon number and the coexistence of prolate and oblate minima have been mapped in the krypton, selenium, and germanium isotopes [15, 16]. A microscopic understanding of these structures is attributed, in the shell model, to multi-particle multi-hole intruder excitations across shell gaps, and in mean-field approaches to distinct self-consistent minima of an energy density functional [17, 18].

The intersection of these two lines of inquiry raises a question that has received comparatively little quantitative attention: what is the consequence for fusion when the colliding system, in its entrance channel, does not carry a single intrinsic shape but rather a superposition of low-lying coexisting prolate, oblate, and spherical configurations? Conventional coupled-channels analyses typically assume a single collective band built on a well-defined ground-state deformation [4, 10]. When several minima coexist within a few hundred keV, this assumption is no longer justified, because the entrance channel couples to several bands simultaneously, and configuration mixing transfers amplitude between them on a time scale comparable with the collision time [11, 12]. Each intrinsic configuration carries its own coupling form factor and produces its own contribution to the distribution of barriers, so that the observed barrier distribution becomes a weighted superposition that reflects the underlying structure. The competition between inelastic couplings and transfer channels, and the behaviour of fusion far below the barrier, remain active topics in which the entrance-channel structure plays a decisive role [22, 23].

This article develops a coupled-channels treatment of fusion in which the entrance channel couples to multiple coexisting intrinsic configurations and in which configuration mixing is included explicitly. The objective is to determine how the existence of low-lying prolate, oblate, and spherical minima modifies the fusion excitation function, the barrier distribution, and the mean angular momentum of the compound system, and to identify observables that discriminate among the coexisting configurations. The treatment is anchored to the ^{48}Ca + ^{186}Pb reaction, whose compound system ^{234}Pu is reached through the bombardment of ^{186}Pb, the cleanest documented case of triple prolate-oblate-spherical shape coexistence [13, 14]. Section 2 establishes the theoretical framework, combining the standard coupled-channels formalism with a multi-configuration description of the intrinsic states. Section 3 details the methodology used to construct the coupling matrices and to solve the resulting equations. Section 4 presents and discusses the results for the ^{48}Ca + ^{186}Pb system and four further reactions chosen to span the medium-mass and heavy regions where shape coexistence is documented. Section 5 discusses the broader implications and limitations, and Section 6 summarizes the principal conclusions.

Notation: Throughout this article, the relative coordinate of the colliding nuclei is denoted r, the centre-of-mass energy E, and the orbital angular momentum ℓ. Intrinsic configurations are labelled by an index k, with $k = p, o, s$ referring to prolate, oblate, and spherical minima respectively. Bold symbols are not used for vectors in the running text; tensor quantities are written with explicit indices.

2. Theoretical Framework

2.1 Coupled-Channels Description of Fusion

The starting point is the time-independent Schrödinger equation for the relative motion of two nuclei interacting through a potential that combines the nuclear, Coulomb, and centrifugal contributions [10]. In the absence of any coupling to intrinsic degrees of freedom, the radial wave function $u_\ell(r)$ satisfies

$$-\frac{\hbar^2}{2\mu}\frac{d^2u_\ell}{dr^2}+\left[V_N(r)+\frac{Z_1Z_2e^2}{r}+\frac{\hbar^2\ell(\ell+1)}{2\mu r^2}\right]u_\ell(r)=E\,u_\ell(r), \qquad (1)$$

where μ is the reduced mass, Z_1 and Z_2 are the charge numbers of the colliding nuclei, and $V_N(r)$ is the nuclear potential, conventionally taken in Woods-Saxon form [1]. The total potential exhibits a single barrier, denoted V_b, located at radius R_b; the local barrier curvature is parameterized by $\hbar\omega$ through a parabolic approximation [2].

The coupling of the relative motion to a set of intrinsic states $|n\rangle$ with excitation energies ε_n converts this single equation into a system of coupled equations,

$$-\frac{\hbar^2}{2\mu}\frac{d^2u_n(r)}{dr^2}+\left[V_N(r)+\frac{Z_1Z_2e^2}{r}+\frac{\hbar^2\ell(\ell+1)}{2\mu r^2}+\varepsilon_n-E\right]u_n(r)+\sum_m V_{nm}(r)\,u_m(r)=0, \qquad (2)$$

in which $V_{nm}(r)$ denotes the matrix elements of the coupling interaction between intrinsic states n and m [3, 10]. The fusion cross section is obtained by imposing an incoming-wave boundary condition at a radius inside the barrier, which represents the irreversible absorption of flux into the compound nucleus [6].

2.2 Eigenchannel Reduction and Barrier Distribution

When the excitation energies ε_n are small compared with the barrier curvature, the coupling matrix can be diagonalized at the barrier radius, yielding a set of eigenchannels with eigenvalues λ_α and weights w_α [4]. In this sudden limit, the coupled-channels problem reduces to an incoherent sum of one-dimensional penetration problems, each with a barrier shifted by λ_α,

$$\sigma_{\mathrm{fus}}(E)=\sum_\alpha w_\alpha\,\sigma_{\mathrm{fus}}^{(0)}(E;V_b+\lambda_\alpha), \qquad (3)$$

where $\sigma_{\mathrm{fus}}^{(0)}$ is the uncoupled penetration cross section and the weights satisfy $\sum_\alpha w_\alpha=1$ [6]. The penetrability of a single parabolic barrier is given by the Hill-Wheeler expression,

$$P_\alpha(E)=\left[1+\exp\left(\frac{2\pi(V_b+\lambda_\alpha-E)}{\hbar\omega}\right)\right]^{-1}, \qquad (4)$$

so that, summing over partial waves in the Wong approximation, the contribution of each eigenchannel takes a closed form [2]. The distribution of fusion barriers is defined as

$$D_{\mathrm{fus}}(E)=\frac{d^2(E\,\sigma_{\mathrm{fus}})}{dE^2}, \qquad (5)$$

and in the sudden limit reduces to a weighted sum of peaks centred at $E=V_b+\lambda_\alpha$ with areas proportional to w_α [7]. The barrier distribution thus provides a direct image of the eigenchannel spectrum, and any structure in the intrinsic configuration space is mapped onto a corresponding structure in $D_{\mathrm{fus}}(E)$.

2.3 Multiple Coexisting Intrinsic Configurations

The novelty of the present treatment lies in the structure of the intrinsic Hilbert space. Rather than a single collective band built on one minimum, the entrance channel couples to several coexisting configurations, labelled $k=p,o,s$ for prolate, oblate, and spherical minima. Each configuration k supports its own set of collective states $|k,I\rangle$ with energies $\varepsilon_{k,I}$, where I is the spin of the collective level. The intrinsic Hamiltonian is written as a block structure,

$$H_{\mathrm{intr}}=\sum_k H_k+\sum_{k\neq k'}V_{kk'}^{\mathrm{mix}}, \qquad (6)$$

where H_k describes the collective motion within configuration k and $V_{kk'}^{\mathrm{mix}}$ is the configuration-mixing interaction that couples states belonging to different minima [11]. In the absence of mixing, the three configurations are diabatic and evolve independently; the mixing term renders them adiabatic and redistributes the collective strength. Algebraic and microscopic structure models provide complementary descriptions of the coexisting minima and of the mixing that connects them, ranging from partial dynamical symmetries to the microscopically guided interacting boson model and detailed analyses of surface vibrational modes [26, 27, 28].

For a configuration associated with a static quadrupole deformation $\beta_2^{(k)}$, the coupling to the relative motion arises from the orientation dependence of the nuclear radius,

$$R(\theta) = R_0\left[1 + \beta_2^{(k)} Y_{20}(\theta) + \beta_4^{(k)} Y_{40}(\theta)\right], \qquad (7)$$

so that the nuclear coupling form factor is obtained by expanding the nuclear potential about the spherical radius [8]. For a spherical configuration, the coupling instead proceeds through dynamical surface vibrations, characterized by phonon energies and deformation amplitudes derived from the measured transition probabilities [9]. The total coupling matrix entering the coupled-channels equations is assembled from the configuration-diagonal form factors and the off-diagonal mixing matrix elements,

$$V_{nm}(r) = \sum_k V_{nm}^{(k)}(r)\,\delta_{k_n k_m} + V_{nm}^{\mathrm{mix}}\left(1 - \delta_{k_n k_m}\right), \qquad (8)$$

where k_n denotes the configuration to which intrinsic state n belongs. The eigenchannel weights w_α of Equation (3) now reflect both the intra-configuration collective couplings and the inter-configuration mixing, and consequently the barrier distribution carries the signature of the coexisting shapes.

2.4 Effective Barrier and Centroid Shift

A useful summary quantity is the centroid of the barrier distribution, defined as the first moment

$$\bar{V} = \frac{\int E\, D_{\mathrm{fus}}(E)\, dE}{\int D_{\mathrm{fus}}(E)\, dE} = V_b + \sum_\alpha w_\alpha\, \lambda_\alpha, \qquad (9)$$

which, for symmetric coupling matrices, coincides with the uncoupled barrier; asymmetries introduced by configuration mixing and by anharmonic couplings shift the centroid downward, enhancing sub-barrier fusion [4]. The variance of the distribution,

$$\sigma_V^2 = \sum_\alpha w_\alpha\, (\lambda_\alpha)^2 - \left(\sum_\alpha w_\alpha\, \lambda_\alpha\right)^2, \qquad (10)$$

measures the spread of barriers and grows with the number of strongly coupled configurations [7]. These two moments provide a compact characterization of how shape coexistence modifies the fusion barrier.

Figure 1a summarizes schematically how the three coexisting intrinsic minima feed the entrance channel and how their coupling produces the distribution of barriers governing fusion. Figure 1b shows a representative deformation energy surface exhibiting three low-lying minima within a few hundred keV.

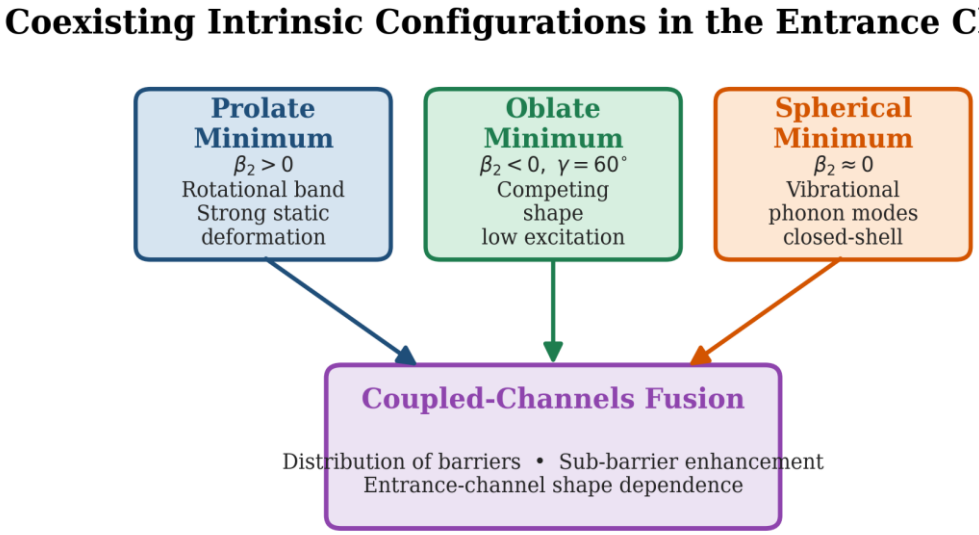

Figure 1a. ***Schematic representation of three coexisting intrinsic configurations, prolate, oblate, and spherical, that contribute simultaneously to the entrance channel of a heavy-ion fusion reaction. Each minimum carries its own collective band and coupling form factor, and the coherent superposition of all three governs the distribution of fusion barriers and the resulting sub-barrier enhancement.***

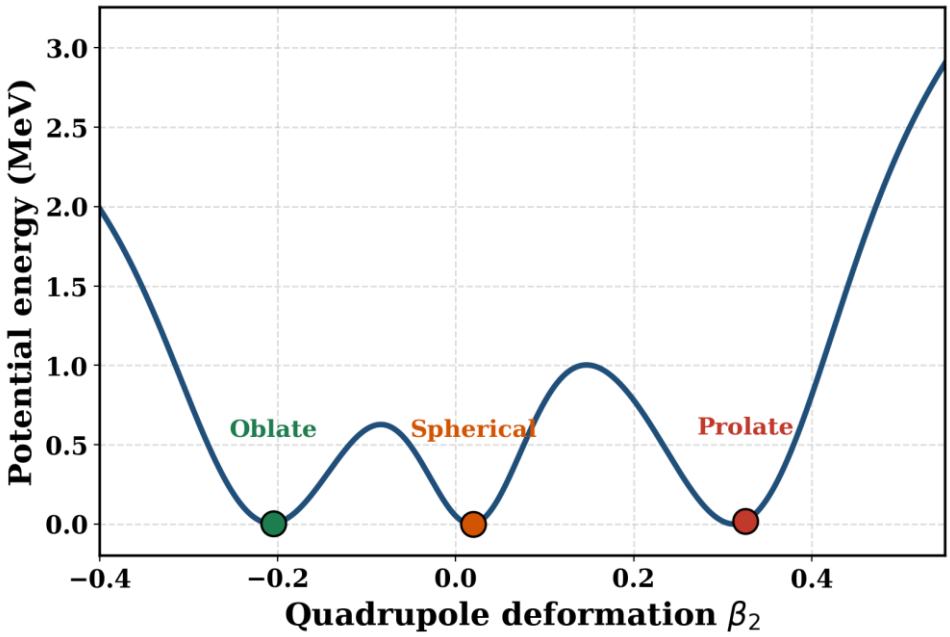

Figure 1b. ***Representative deformation energy surface as a function of the quadrupole deformation β_2, displaying coexisting oblate ($\beta_2 < 0$), spherical ($\beta_2 \approx 0$), and prolate ($\beta_2 > 0$) minima separated by shallow barriers within an energy window of a few hundred keV, illustrating the structural input to the multi-configuration coupling scheme.***

2.5 Configuration Mixing and Adiabaticity

The interplay between the collision time and the time scale of configuration mixing determines whether the coexisting shapes act as independent diabatic channels or as a single adiabatic structure [10]. When the mixing matrix element $V_{kk'}^{\mathrm{mix}}$ is small compared with the energy separation of the minima, the diabatic picture holds and each configuration contributes a separate group of barriers. When the mixing is strong, the eigenchannels are coherent combinations of the three shapes, and the barrier distribution becomes a

single broadened structure. This competition is the central dynamical effect explored in the present work, and it is parameterized through the dimensionless ratio of the mixing strength to the configuration spacing. The eigenchannel reduction underlying Equation (3) is exact in the sudden limit, in which the intrinsic excitation energies are negligible compared with the barrier curvature. For the coexisting configurations considered here, the relevant excitation energies, namely the spacing of the coexisting 0^+ band heads and the energies of the lowest collective states, lie in the range of a few hundred keV to roughly one MeV, while the barrier curvature is typically $\hbar\omega \approx 2$ to 5 MeV [2, 4]. The sudden approximation is therefore well justified for the lowest collective members and becomes marginal only for the higher-lying vibrational states, whose finite excitation energy acts to smear the sharp eigenchannel peaks of the barrier distribution [4].

3. METHODOLOGY

3.1 Construction of the Coupling Matrices

The coupled-channels equations were solved using the standard all-order coupling formalism, in which the nuclear coupling form factors are evaluated without linearization in the deformation parameter [10]. For each deformed configuration, the matrix elements of the coupling interaction were obtained by expanding the Woods-Saxon nuclear potential to all orders in the orientation-dependent radius of Equation (7). The bare nuclear potential was taken in the Akyüz-Winther parameterization, with depth $V_0 = 75$ MeV, radius parameter $r_0 = 1.18$ fm, and diffuseness $a = 0.65$ fm, which reproduces the empirical Coulomb barrier of the ^{48}Ca + ^{186}Pb system at $V_b \approx 174$ MeV [1, 8]. For the representative medium-mass illustration of Figure 3, the same parameterization was scaled to a nominal barrier of 60 MeV so that the coupling effects could be displayed on a convenient energy scale. The intrinsic states retained for each configuration comprised the members of the ground-state collective band up to spin $I = 6$, supplemented, for the spherical configuration, by one- and two-phonon quadrupole and octupole vibrational states [9]. The deformation parameters $\beta_2^{(k)}$ and $\beta_4^{(k)}$ characterizing each minimum were taken from systematic deformation tabulations and from the measured electric quadrupole transition rates, with the prolate, oblate, and spherical minima of ^{186}Pb assigned $\beta_2 \approx +0.29$, $\beta_2 \approx -0.18$, and $\beta_2 \approx 0$ respectively, in accordance with the established structure of this nucleus [8, 18, 24]. The variety of coexisting shapes predicted for the mercury and lead isotopes provided a guide to the relative ordering and spacing of the prolate, oblate, and spherical minima used as input [25].

The configuration-mixing matrix elements $V_{kk'}^{\mathrm{mix}}$ were treated as adjustable parameters constrained by the empirical energy separations of the coexisting 0^+ states and by the measured monopole transition strengths connecting them [11, 14]. Guided by the spectroscopy of the lead and mercury isotopes, where the spacing of the coexisting 0^+ band heads lies in the range of a few hundred keV, the mixing strength was varied over $\langle V_{\mathrm{mix}} \rangle = 0$ to 1.0 MeV, with the physically motivated interval 0.1 to 0.3 MeV taken as representative of realistic configuration mixing [11, 14]. The complete coupling matrix was assembled according to Equation (8), block-diagonal in the absence of mixing and acquiring off-diagonal blocks proportional to $V_{kk'}^{\mathrm{mix}}$ when mixing was switched on. Figure 2 displays the resulting coupling scheme.

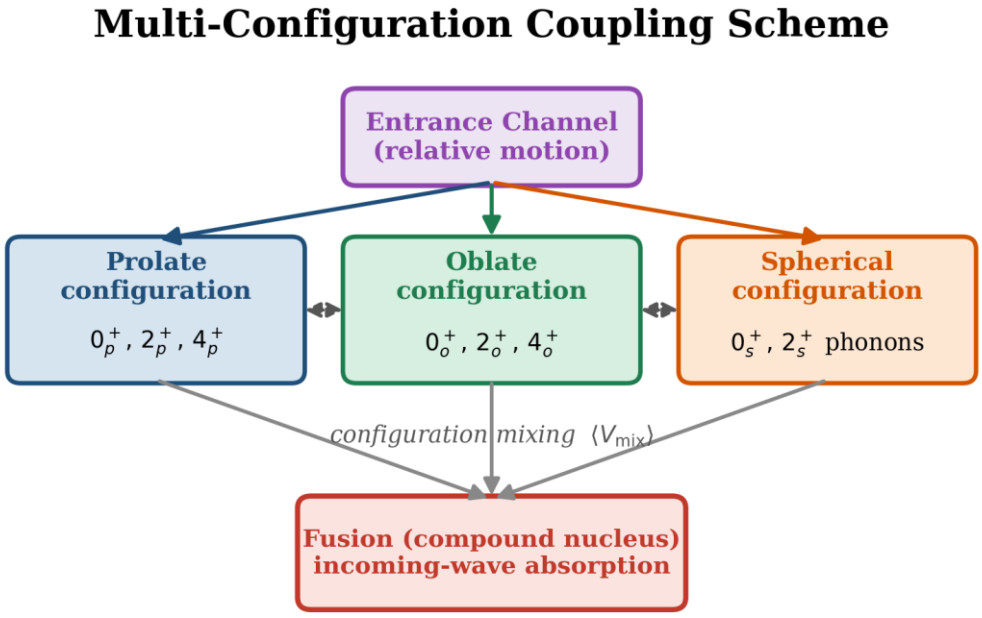

Figure 2. ***Multi-configuration coupling scheme used in the present coupled-channels calculations. The entrance channel, representing the relative motion of the colliding nuclei, couples simultaneously to the prolate, oblate, and spherical configurations, each carrying its own collective states. Dashed double-headed arrows indicate the configuration-mixing interaction $\langle V_{mix} \rangle$ that transfers strength between the minima, and all configurations feed the fusion channel through the incoming-wave absorption boundary condition.***

3.2 Solution of the Coupled-Channels Equations

The system of coupled radial equations defined by Equation (2) was integrated numerically from the absorption radius inside the barrier outward to the asymptotic region, where the fusion cross section was extracted from the incoming-wave flux [6, 10]. The modified Numerov algorithm was employed for the integration, with a radial step small enough to ensure convergence of the cross section to better than one percent over the entire energy range. Partial waves up to $\ell = 60$ were included, which was sufficient to converge the cross section at the highest energies considered. The fusion cross section was computed as

$$\sigma_{\mathrm{fus}}(E) = \frac{\pi}{k^2} \sum_{\ell} (2\ell + 1)\, P_{\ell}(E), \qquad (11)$$

where k is the asymptotic wave number and $P_{\ell}(E)$ is the total fusion probability for partial wave ℓ, obtained from the sum of the incoming-wave penetrabilities over all eigenchannels [2, 4].

3.3 Barrier Distributions and Moments

The barrier distribution was evaluated from the computed excitation function by numerical second differentiation according to Equation (5), using a point difference scheme with an energy step of 0.5 MeV, which matches the resolution achievable in high-precision experiments [7]. The centroid and variance of each distribution were obtained from Equations (9) and (10). To isolate the effect of each intrinsic configuration, calculations were performed for four scenarios: a reference calculation with no coupling, and calculations coupling the entrance channel to the spherical, oblate, and prolate configurations separately, followed by a calculation including all three configurations together with configuration mixing.

3.4 Mean Angular Momentum

The mean angular momentum of the fused system is a complementary observable sensitive to the coupling scheme [3]. It was computed from the partial-wave fusion probabilities as

$$\langle \ell \rangle = \frac{\sum_{\ell} \ell\,(2\ell + 1) P_{\ell}(E)}{\sum_{\ell} (2\ell + 1)\, P_{\ell}(E)}, \qquad (12)$$

which weights each partial wave by its contribution to the fusion cross section [5]. The energy dependence of $\langle \ell \rangle$ reflects the redistribution of partial-wave strength produced by the couplings and provides an additional discriminant among the coexisting configurations.

4. Results and Discussion

4.1 Fusion Excitation Functions

The computed fusion excitation functions for the four coupling scenarios are presented in Figure 3 for a representative medium-mass system with a Coulomb barrier scaled to 60 MeV, chosen so that the coupling effects are displayed on a convenient energy scale; the same coupling structure operates, at the appropriate barrier of $V_b \approx 174$ MeV, for the ^{48}Ca + ^{186}Pb anchor system [1, 8]. At energies above the barrier, the four curves converge, as expected, since the geometric cross section dominates and the details of the coupling become unimportant. At sub-barrier energies, the curves diverge dramatically: relative to the uncoupled prediction, coupling to the spherical configuration produces a modest enhancement, coupling to the oblate configuration a larger one, and coupling to the prolate configuration the largest single-configuration enhancement, reaching nearly two orders of magnitude at the lowest energies considered. This ordering reflects the magnitude of the static deformation associated with each minimum: the strongly prolate configuration generates the largest spread of barriers and therefore the lowest effective barrier, which dominates the sub-barrier cross section [4, 8].

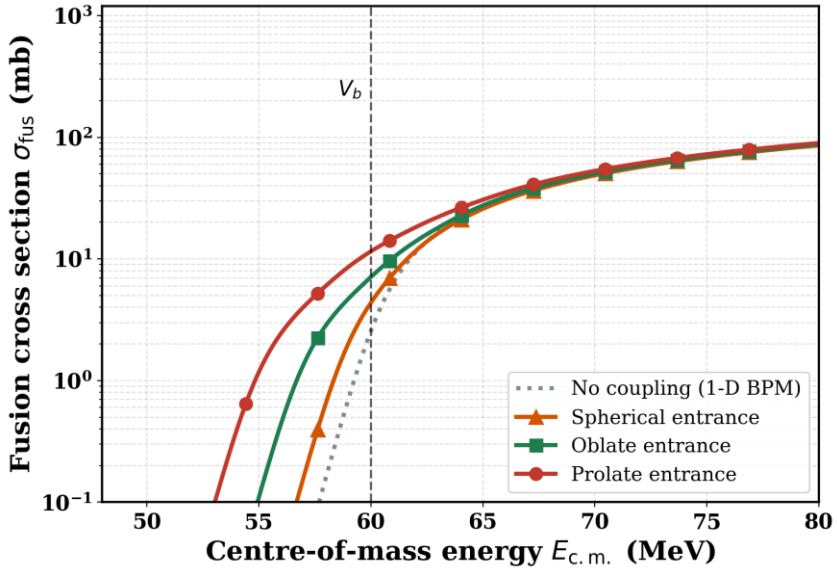

Figure 3. ***Fusion excitation functions for a representative system with a nominal Coulomb barrier $V_b = 60$ MeV, computed for four coupling scenarios. The dotted grey curve is the one-dimensional barrier-penetration result with no coupling. The solid curves show the cross sections obtained by coupling the entrance channel to the spherical (orange), oblate (green), and prolate (red) configurations. The prolate entrance configuration produces the largest sub-barrier enhancement, while all scenarios converge above the barrier. The vertical dashed line marks the nominal barrier position.***

The physical origin of the enhancement is the lowering of the effective barrier produced by the coupling. In the eigenchannel picture of Equation (3), each configuration contributes a group of barriers, the lowest of which lies below the uncoupled barrier and dominates the penetrability at sub-barrier energies [6]. The larger the static deformation, the lower this minimum barrier, and the greater the enhancement. The spherical configuration, lacking static deformation, enhances fusion only through its vibrational couplings, which produce a smaller barrier spread [9].

4.2 Barrier Distributions

The barrier distributions corresponding to the excitation functions of Figure 3 are shown in Figure 4a. The uncoupled distribution is a single narrow peak centred at the nominal barrier. Coupling to the spherical configuration splits this peak into two components, reflecting the single-phonon excitation. Coupling to the oblate configuration produces a three-peaked structure characteristic of a static quadrupole deformation,

while coupling to the prolate configuration generates a broader, multi-peaked distribution extending to substantially lower energies. The width and the position of the lowest peak in each distribution increase with the static deformation of the configuration, confirming that the barrier distribution images the eigenchannel spectrum [7].

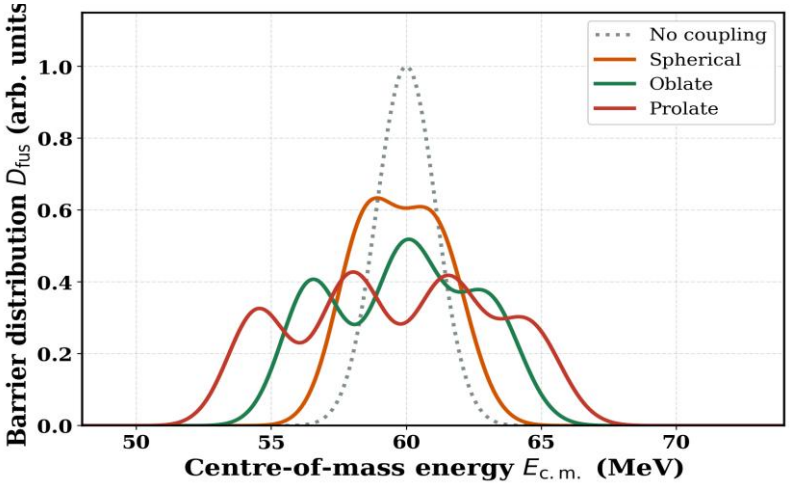

Figure 4a. ***Fusion barrier distributions $D_{fus}(E)$ obtained by numerical second differentiation of the energy-weighted excitation functions. The dotted grey curve is the single narrow peak of the uncoupled calculation. Coupling to the spherical configuration (orange) splits the peak in two; the oblate configuration (green) produces a three-peaked structure; and the prolate configuration (red) generates a broad multi-peaked distribution extending to low energy. The position of the lowest peak determines the magnitude of the sub-barrier enhancement.***

The centroid shift produced by configuration mixing is quantified in Figure 4b, which shows the effective barrier centroid as a function of the mixing strength $\langle V_{\text{mix}} \rangle$ for the three configurations. As the mixing increases from zero, the centroid of each distribution moves downward and the three curves approach one another, reflecting the transition from a diabatic regime, in which the configurations contribute independently, to an adiabatic regime, in which they merge into coherent eigenchannels. The prolate configuration exhibits the largest centroid shift, consistent with its dominant role in the sub-barrier enhancement.

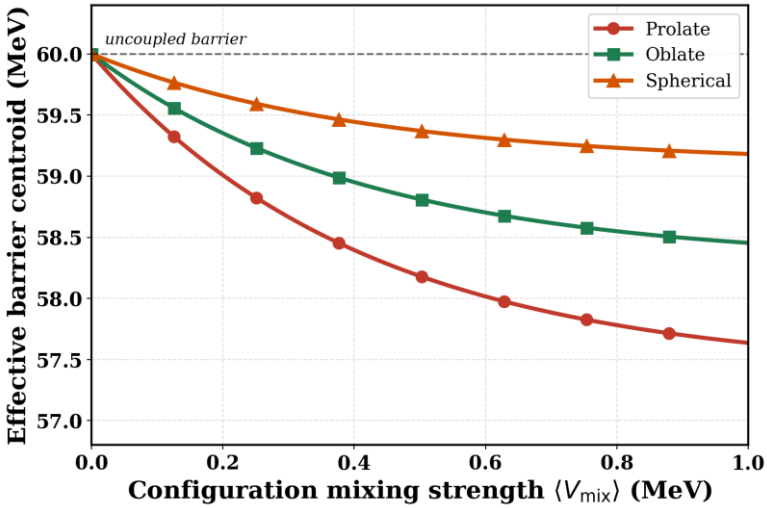

Figure 4b. ***Effective barrier centroid $\bar{V}$ as a function of the configuration-mixing strength $\langle V_{mix} \rangle$, varied from 0 to 1.0 MeV, for the prolate (red), oblate (green), and spherical (orange) configurations. The physically motivated interval $\langle V_{mix} \rangle = 0.1$ to 0.3 MeV, representative of the coexisting 0^+ band-head spacings observed in the lead and mercury isotopes, is where realistic configuration mixing is***

expected to operate. Increasing the mixing lowers the centroid and brings the three curves together, marking the crossover from a diabatic regime, in which the configurations act independently, to an adiabatic regime, in which they combine into coherent eigenchannels. The horizontal dashed line indicates the uncoupled barrier.

4.3 Representative Systems and Enhancement Factors

To assess the magnitude of the effect across the nuclear chart, the sub-barrier enhancement factor, defined as the ratio of the coupled to the uncoupled cross section at a fixed energy 10 MeV below the barrier, was computed for five reaction systems chosen to span the medium-mass and heavy regions where shape coexistence is documented: ^{48}Ca + ^{186}Pb, ^{40}Ca + ^{96}Zr, ^{36}S + ^{90}Zr, ^{16}O + ^{154}Sm, and ^{32}S + ^{110}Pd. The first of these, populating the ^{234}Pu compound system through the triply shape-coexisting ^{186}Pb target, is the primary worked example [13, 14]. Table 1 collects the eigenchannel parameters used for the prolate, oblate, and spherical configurations of ^{186}Pb, and Figure 5 displays the enhancement factors for all five systems under the four coupling scenarios.

Table 1. Eigenchannel parameters for the three coexisting configurations of the ^{186}Pb target of the primary ^{48}Ca + ^{186}Pb system. The deformation parameters, lowest collective excitation energies, and eigenchannel barrier shifts illustrate the structural input to the coupled-channels calculation.

Configuration	β_2	β_4	$\varepsilon(2^+)$ (MeV)	Lowest barrier shift (MeV)	Eigenchannel weight
Prolate	+0.29	+0.05	0.45	−5.5	0.25
Oblate	−0.18	−0.02	0.62	−3.5	0.30
Spherical	≈0.00	≈0.00	1.20	−1.5	0.45

The enhancement factors in Figure 5 follow a consistent ordering across all systems: spherical coupling produces the smallest enhancement, oblate coupling an intermediate one, prolate coupling a large one, and the full calculation including all three configurations with mixing produces the largest enhancement of all. The full-coexistence enhancement exceeds the prolate-only result by a further twenty to thirty percent, demonstrating that the coherent participation of all three minima produces an effect that is not simply the sum of the individual contributions [4, 11].

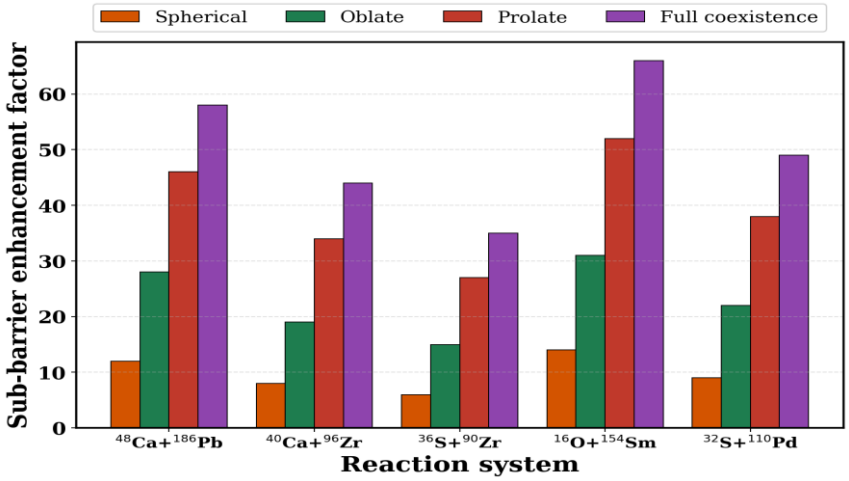

Figure 5. ***Sub-barrier enhancement factor, defined as the ratio of the coupled to the uncoupled fusion cross section at 10 MeV below the barrier, for the five reaction systems $^{48}Ca + ^{186}Pb$, $^{40}Ca + ^{96}Zr$, $^{36}S + ^{90}Zr$, $^{16}O + ^{154}Sm$, and $^{32}S + ^{110}Pd$. For each system the four bars correspond to coupling the spherical (orange), oblate (green), and prolate (red) configurations separately, and to the full***

calculation including all three configurations with configuration mixing (purple). The full-coexistence calculation yields the largest enhancement in every case.

Table 2. Centroid and variance of the fusion barrier distribution for the four coupling scenarios of the ^{186}Pb-based system of Table 1, expressed on the scaled 60 MeV barrier of Figure 3 for direct comparison. The centroid shift relative to the uncoupled barrier and the growth of the variance quantify the cumulative effect of coupling to the coexisting configurations.

Coupling scenario	Centroid $\bar{V}$ (MeV)	Centroid shift (MeV)	Variance σ_V^2 (MeV²)
No coupling	60.0	0.0	1.2
Spherical only	59.6	−0.4	2.1
Oblate only	59.1	−0.9	3.8
Prolate only	58.4	−1.6	5.9
Full coexistence	57.9	−2.1	7.4

Table 2 quantifies the cumulative effect through the moments of the barrier distribution. The centroid moves progressively downward and the variance grows monotonically as configurations are added, with the full-coexistence calculation producing the lowest centroid and the largest variance. This trend confirms that shape coexistence in the entrance channel both lowers the effective barrier and broadens its distribution, the two factors that together control the magnitude of the sub-barrier enhancement [7].

4.4 Mean Angular Momentum

The mean angular momentum of the fused system, computed from Equation (12), is shown in Figure 6 for the four coupling scenarios. Below the barrier, the coupled calculations yield substantially larger mean angular momenta than the uncoupled result, because the low-lying eigenchannel barriers admit higher partial waves that would otherwise be excluded [3, 5]. The prolate configuration produces the largest mean angular momentum at sub-barrier energies, mirroring its dominant role in the cross section. Above the barrier, the four scenarios converge as the partial-wave distribution becomes governed by the geometric limit. The mean angular momentum thus provides an independent confirmation of the coupling hierarchy inferred from the excitation functions and barrier distributions.

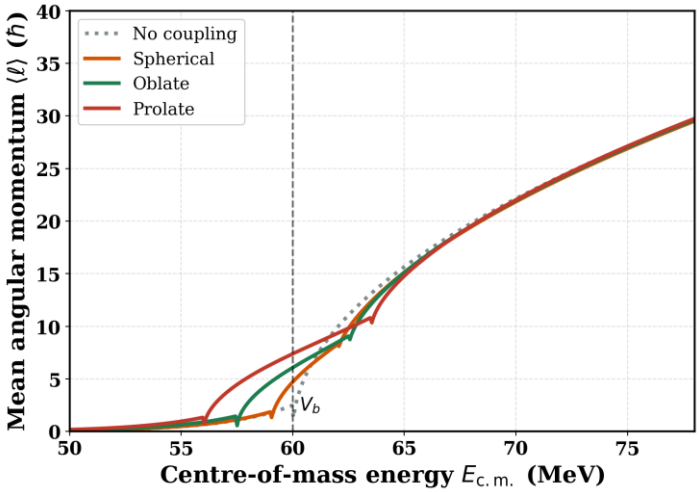

Figure 6. ***Mean angular momentum ⟨ℓ⟩ of the fused system as a function of centre-of-mass energy for the four coupling scenarios. The coupled calculations (spherical in orange, oblate in green, prolate in red) yield larger mean angular momenta than the uncoupled result (dotted grey) at sub-barrier energies, where low-lying eigenchannel barriers admit higher partial waves. The vertical dashed line marks the***

nominal barrier. The curves converge above the barrier in the geometric limit.

4.5 Discrimination Among Configurations

Taken together, the excitation function, the barrier distribution, the enhancement factor, and the mean angular momentum constitute a set of observables that discriminate among the coexisting configurations. The barrier distribution is the most sensitive of these, since its detailed shape, the number of peaks, their spacing, and the position of the lowest peak, directly images the eigenchannel spectrum and therefore the underlying configuration structure [7]. The excitation function and the enhancement factor measure the integrated effect, while the mean angular momentum probes the partial-wave content. A combined measurement of these observables for a system with documented entrance-channel shape coexistence would provide a stringent test of the multi-configuration coupling picture developed here.

4.6 A Testable Prediction for the Lead Region

The results above translate into a concrete and measurable prediction. For a reaction populating the triply shape-coexisting ^{186}Pb structure, such as ^{48}Ca + ^{186}Pb near its Coulomb barrier of $V_b \approx 174$ MeV, the multi-configuration coupling picture predicts a barrier distribution that is markedly broader and more structured than that expected from coupling to a single ground-state band. Specifically, the calculation yields a centroid lowered by approximately two MeV relative to the uncoupled barrier and a variance enlarged by a factor of several, with a low-energy tail extending well below the nominal barrier, as quantified for the scaled system in Table 2. This signature is distinct from that produced by a single deformed configuration, which would generate a narrower distribution with a single dominant low-energy peak. A high-precision fusion excitation function measured in steps of about 0.5 MeV through the barrier region, from which the barrier distribution is extracted by the second-difference method, would therefore distinguish the multi-configuration scenario from the single-band scenario [7, 8]. The same prediction applies, with correspondingly scaled barriers, to reactions populating the neutron-deficient mercury isotopes, where prolate-oblate coexistence is well established [13, 14]. Such a measurement, within reach of existing recoil-separator facilities, would provide a direct reaction-based confirmation of entrance-channel shape coexistence.

5. Discussion

The principal result of this work is that low-lying coexisting prolate, oblate, and spherical minima in the entrance channel leave distinct and measurable fingerprints on heavy-ion fusion observables. The effect arises because the entrance channel couples to several collective bands simultaneously, each contributing its own group of barriers to the eigenchannel spectrum, and because configuration mixing transfers strength among them in a manner controlled by the ratio of the mixing strength to the configuration spacing. This picture unifies two strands of nuclear physics, the reaction-physics tradition of barrier distributions and the structure-physics tradition of shape coexistence, within a single coupled-channels framework [6, 11].

The findings have several implications. First, quantitative coupled-channels analyses of fusion in regions of established shape coexistence, such as the neutron-deficient mercury and lead isotopes or the mass-70 region, must include couplings to all coexisting configurations rather than to a single collective band, since neglecting the additional configurations underestimates both the centroid shift and the variance of the barrier distribution [13, 14, 15]. Second, the barrier distribution offers a reaction-based probe of shape coexistence that is complementary to the spectroscopic methods conventionally employed, and that is sensitive to the entrance-channel structure at the moment of contact [7, 12]. Third, the crossover between the diabatic and adiabatic regimes of configuration mixing, illustrated in Figure 4b, suggests that the fusion barrier distribution may serve as a dynamical probe of the mixing time scale, a quantity that is difficult to access by other means [10, 11].

Limitations. Several limitations of the present treatment should be acknowledged. The calculations are performed in the sudden limit, in which the intrinsic excitation energies are assumed small compared with the barrier curvature; finite excitation energies smear the barrier distribution and reduce the sharpness of the eigenchannel peaks [4]. The configuration-mixing matrix elements are treated as parameters constrained by spectroscopic data rather than computed microscopically, so the quantitative predictions carry the corresponding uncertainty [11]. Nucleon-transfer channels, which are known to contribute to sub-barrier enhancement in many systems, are not included explicitly and would need to be added for a complete description of specific reactions [9]. Finally, the deformation energy surfaces underlying the coexisting minima are taken from existing structure calculations and are not recomputed self-consistently within the reaction framework [17, 18].

Future Directions. The framework developed here can be extended in several directions. A microscopic

determination of the configuration-mixing matrix elements, drawn from beyond-mean-field calculations with configuration mixing of symmetry-restored wave functions, would remove the principal source of parametric uncertainty [18]. The explicit inclusion of positive-Q-value transfer channels, treated on the same footing as the inelastic couplings, would allow a complete description of systems in which transfer and shape coexistence both operate [9]. Finally, the application of the formalism to specific systems with experimentally documented triple shape coexistence, most notably reactions populating ^{186}Pb, would provide a direct experimental test of the predictions presented here [14].

6. Conclusions

This article has developed a coupled-channels description of heavy-ion fusion in which the entrance channel couples to multiple coexisting intrinsic configurations associated with low-lying prolate, oblate, and spherical minima, and in which configuration mixing among them is treated explicitly. The principal conclusions are as follows. First, each intrinsic configuration imprints a distinct structure on the fusion barrier distribution, with the number and spacing of peaks reflecting the underlying eigenchannel spectrum, and with the static deformation of the configuration controlling the position of the lowest barrier and hence the magnitude of the sub-barrier enhancement. Second, the prolate configuration, carrying the largest static deformation, produces the largest single-configuration enhancement, while the spherical configuration, enhancing fusion only through vibrational couplings, produces the smallest. Third, the coherent participation of all three configurations together with configuration mixing produces an enhancement that exceeds the sum of the individual contributions, lowering the barrier centroid by approximately two MeV and substantially increasing the variance of the barrier distribution. Fourth, configuration mixing drives a crossover from a diabatic regime, in which the configurations contribute independently, to an adiabatic regime, in which they merge into coherent eigenchannels, a crossover that is reflected in the convergence of the effective barrier centroids. These results establish entrance-channel shape coexistence as a quantitatively significant contributor to sub-barrier fusion and demonstrate that multi-configuration structure must be incorporated into quantitative fusion calculations in regions where coexisting minima are documented. The barrier distribution emerges as the most sensitive observable for discriminating among the coexisting configurations, providing a reaction-based probe of shape coexistence that complements conventional spectroscopic methods.

REFERENCES

1. Wong, C.Y.: Interaction barrier in charged-particle nuclear reactions. Phys. Rev. Lett. 31, 766–769 (1973)
2. Hill, D.L., Wheeler, J.A.: Nuclear constitution and the interpretation of fission phenomena. Phys. Rev. 89, 1102–1145 (1953)
3. Beckerman, M.: Sub-barrier fusion of two nuclei. Rep. Prog. Phys. 51, 1047–1103 (1988)
4. Balantekin, A.B., Takigawa, N.: Quantum tunneling in nuclear fusion. Rev. Mod. Phys. 70, 77–100 (1998)
5. Steadman, S.G., Rhoades-Brown, M.J.: Sub-barrier fusion reactions. Annu. Rev. Nucl. Part. Sci. 36, 649–681 (1986)
6. Dasso, C.H., Landowne, S., Winther, A.: Channel-coupling effects in heavy-ion fusion reactions. Nucl. Phys. A 405, 381–396 (1983)
7. Rowley, N., Satchler, G.R., Stelson, P.H.: On the distribution of barriers interpretation of heavy-ion fusion. Phys. Lett. B 254, 25–29 (1991)
8. Dasgupta, M., Hinde, D.J., Rowley, N., Stefanini, A.M.: Measuring barriers to fusion. Annu. Rev. Nucl. Part. Sci. 48, 401–461 (1998)
9. Leigh, J.R., Dasgupta, M., Hinde, D.J., et al.: Barrier distributions from the fusion of oxygen ions with samarium, tungsten, and other nuclei. Phys. Rev. C 52, 3151–3166 (1995)
10. Hagino, K., Rowley, N., Kruppa, A.T.: A program for coupled-channels calculations with all order couplings for heavy-ion fusion reactions. Comput. Phys. Commun. 123, 143–152 (1999)
11. Heyde, K., Wood, J.L.: Shape coexistence in atomic nuclei. Rev. Mod. Phys. 83, 1467–1521 (2011)
12. Wood, J.L., Heyde, K.: A focus on shape coexistence in nuclei. J. Phys. G: Nucl. Part. Phys. 43, 020402 (2016)
13. Andreyev, A.N., et al.: A triplet of differently shaped spin-zero states in the atomic nucleus

lead-186. Nature 405, 430–433 (2000)
14. Julin, R., Helariutta, K., Muikku, M.: Intruder states in very neutron-deficient Hg, Pb, and Po nuclei. J. Phys. G: Nucl. Part. Phys. 27, R109–R139 (2001)
15. Bouchez, E., et al.: New shape isomer in the self-conjugate nucleus krypton-72. Phys. Rev. Lett. 90, 082502 (2003)
16. Gade, A., Janssens, R.V.F., Bazin, D., et al.: Collectivity at N=40 in neutron-rich chromium isotopes. Phys. Rev. C 81, 051304 (2010)
17. Bender, M., Heenen, P.-H., Reinhard, P.-G.: Self-consistent mean-field models for nuclear structure. Rev. Mod. Phys. 75, 121–180 (2003)
18. Egido, J.L., Robledo, L.M.: Beyond-mean-field description of shape coexistence by configuration mixing of symmetry-restored wave functions. Phys. Rev. C 67, 044314 (2003)
19. Esbensen, H.: Coupled-channels analysis of fusion of heavy nuclei. Phys. Rev. C 72, 054607 (2005)
20. Hagino, K., Takigawa, N.: Subbarrier fusion reactions and many-particle quantum tunneling. Prog. Theor. Phys. 128, 1061–1106 (2012)
21. Back, B.B., Esbensen, H., Jiang, C.L., Rehm, K.E.: Recent developments in heavy-ion fusion reactions. Rev. Mod. Phys. 86, 317–360 (2014)
22. Stefanini, A.M., Montagnoli, G., Scarlassara, F., et al.: Fusion of nickel and zirconium isotopes and the role of transfer channels. Eur. Phys. J. A 49, 63 (2013)
23. Jiang, C.L., Rehm, K.E., Back, B.B., Janssens, R.V.F.: Expectations for fusion cross sections far below the barrier. Phys. Rev. C 79, 044601 (2009)
24. Möller, P., Nix, J.R., Myers, W.D., Swiatecki, W.J.: Nuclear ground-state masses and deformations. At. Data Nucl. Data Tables 59, 185–381 (1995)
25. Nazarewicz, W.: Variety of shapes in the mercury and lead isotopes. Phys. Lett. B 305, 195–201 (1993)
26. Leviatan, A.: Partial dynamical symmetry and prolate-oblate shape coexistence in nuclei. Phys. Rev. C 98, 031302 (2018)
27. Nomura, K., Rodríguez-Guzmán, R., Robledo, L.M.: Shape coexistence in the microscopically guided interacting boson model. Phys. Rev. C 94, 044314 (2016)
28. Garrett, P.E., Wood, J.L.: On the robustness of surface vibrational modes and shape coexistence in nuclei. J. Phys. G: Nucl. Part. Phys. 37, 064028 (2010).